THE VULCAN PHOTOMETER: A DEDICATED PHOTOMETER FOR EXTRASOLAR PLANET SEARCHES

William J. Borucki[1], Douglas Caldwell, David G. Koch, Larry D. Webster
(NASA Ames Research Center, Moffett Field, CA 94035)
Jon M. Jenkins (SETI Institute, Mountain View, CA 94043)
Zoran Ninkov (Rochester Institute of Technology, Rochester, NY 14623)
Robert Showen (Raytheon Systems Company, Moffett Field, CA 94035

Abstract:
A small CCD photometer dedicated to the detection of extrasolar planets has been developed and put into operation at Mt. Hamilton, California. It simultaneously monitors 6000 stars brighter than 13th magnitude in its 49 square-degree field of view. Observations are conducted all night every clear night of the year. A single field is monitored at a cadence of eight images per hour for a period of about three months. When the data are folded for the purpose of discovering low amplitude transits, transit amplitudes of 1% are readily detected This precision is sufficient to find jovian-size planets orbiting solar-like stars, which have signal amplitudes from 1% to 2% depending on the inflation of the planet's atmosphere and the size of the star. An investigation of possible noise sources indicates that neither star field crowding, scintillation noise, nor photon shot noise are the major noise sources for stars brighter than visual magnitude 11.6.

Over one hundred variable stars have been found in each star field. About fifty of these stars are eclipsing binary stars, several with transit amplitudes of only a few percent. Three stars that showed only primary transits were examined with high-precision spectroscopy. Two were found to be nearly identical stars in binary pairs orbiting at double the photometric period. Spectroscopic observations showed the third star to be a high mass-ratio single-lined binary. On November 22, 1999 the transit of a planet orbiting HD209458 was observed and the predicted amplitude and immersion times were confirmed. These observations show that the photometer and the data reduction and analysis algorithms have the necessary precision to find companions with the expected area ratio for jovian-size planets orbiting solar-like stars.

INTRODUCTION:

A knowledge of other planetary systems that includes information on the number, size, mass, and spacing of the planets around a variety of star types is needed to deepen our understanding of planetary system formation and processes that give rise to their final configurations. Recent discoveries show that many planetary systems are quite different from the solar system in that they possess giant planets in short-period orbits and that they often have highly eccentric orbits. Current theories predict that the size of the atmospheres of the short-period planets will vary with the mass of the planet and the size of the orbital semi-major axis because of the intense stellar insolation. To obtain

[1] Email address: wborucki@mail.arc.nasa.gov

information on the size, mass, density, and orbital parameters of the giant-inner planets and to develop the statistical dependencies of these, it is necessary to observe many of these objects for a variety of stellar spectral types and stellar compositions. Similarly the discoveries that binary stars also have low mass companions (Cochran et al.1997, Butler et al.1997), demand that many more objects must be discovered and studied so that the differences between planetary systems in single stars versus multiple star systems can be understood.

The current method of discovering giant planets uses high precision Doppler velocity measurements of the shifting positions of a star's spectrum over a time interval of one to two planetary orbital periods. To detect planetary mass objects, the measurements of the wavelength shift must be made with a relative precision of a few parts per hundred million. To obtain this level of precision requires the photon shot noise to be extremely small which in turn, demands the use of very large aperture telescopes, such as the Keck instrument in Hawaii. Since only a few percent of the target stars show the presence of planets, this is a time consuming and expensive process. A much less expensive method of obtaining statistical information on inner planets is to use small photometric telescopes to identify those stars with planetary-size companions and then determine their mass and density from Doppler velocity observations using a large aperture telescope. To test this approach, we have constructed a small photometer and have begun observations at the Lick Observatory on Mt. Hamilton. This paper describes the photometer, provides a sampling of some stellar systems showing the presence of very low amplitude transits, and presents subsequent spectral and Doppler velocity observations of these stars.

PRECISION NEEDED TO FIND EXTRASOLAR PLANETS

Transits of planets the size of Jupiter and Saturn produce a 1% reduction in the brightness of a G2 main sequence star like our Sun. For planets like 51Peg B that are at distance of 0.05 AU from their star, the large heat flux from the nearby star is expected to inflate the atmosphere so that the planetary radius could increase to as much as 1.9 times that of Jupiter Rj for a planet with an age of 1 Gyr or to a value of 1.3 Rj for a planet with an age of 8 Gyr (Guillot et al., 1996). Thus the signal from mature, close-in planets is expected to be up to 70% larger than that of Jupiter. The expected signal amplitude for such planets also depends on the size of the star they orbit. For main sequence stars as large as spectral type F0, a jovian-size planet would produce a flux change of 0.45 %. Flux reductions of 3% to 5% are expected for main sequence stars of spectral class M0. See Table 1.

Table 1. Signal Size vs. Stellar Type for Jovian-size Planets and Main Sequence Stars

Stellar Type	Stellar Radius (R_0) (Lang, 1992)	Signal Amplitude for Jovian-size Planet (Ap/A_*)	Signal Amplitude for Close-in Planet with an Inflated Atmosphere
A0	2.4	1.8×10^{-3}	$.31 \times 10^{-2}$
A5	1.7	3.5×10^{-3}	$.60 \times 10^{-2}$
F0	1.5	4.5×10^{-3}	$.76 \times 10^{-2}$
F5	1.3	6.0×10^{-3}	1.0×10^{-2}
G0	1.1	8.3×10^{-3}	1.4×10^{-2}
G5	0.92	11.9×10^{-3}	2.0×10^{-2}
K0	0.85	14.0×10^{-3}	2.4×10^{-2}
K5	0.72	19.5×10^{-3}	3.3×10^{-2}
M0	0.6	28.1×10^{-3}	4.8×10^{-2}

Signals with amplitudes of 1% or greater can be detected when special care is taken to minimize the errors introduced by the atmosphere and the instrumentation. Nevertheless, three or more transits that demonstrate a consistency in period, depth, and duration must be observed to have confidence in the reality of any detection.

For sufficiently bright stars, the precision of ground based photometry is generally limited by atmospheric effects such as extinction and scintillation (Young, 1974, Dravins et al., 1998), but is also greatly affected by telescope tracking and by detector noise. On photometric nights and when sufficient care is taken, it is possible to obtain measurements with an hour-to-hour relative precision of 0.1 to 0.3% (Olsen, 1977, Frandsen et. al., 1989, Gilliland and Brown, 1992).

Note that in doing relative photometry, each target star is measured relative to a group of reference stars measured simultaneously with the target star and in the same field of view as the target star. The only measurements that we report here are the changes in the relative brightness of the target star (compared to its reference stars) that occur over a period of a few hours. The measurements of the relative brightness of all 6000 stars are repeated every 7.5 minutes throughout the night for every clear night during a period of several months. To avoid repositioning the photometer, only one star field is observed each three month period. By observing several transits and folding the data so that the transits align, we have been able to monitor many stars with an hour-to-hour relative precision of about 0.1%. Hence 10-σ detections are possible for jovian-size planets and 7-σ detections are expected for Saturn-size planets.

EXPECTED DETECTION RATE

The expected detection rate per star can be estimated from;

$$R = Pd*Pp*Pa*P_3, \quad (1)$$

where Pd is probability that a field star is a dwarf, Pp is the probability that a dwarf star has a planet with a 3 to 6 day orbit, Pa is the probability that the planetary orbit is aligned close enough to the line of sight to produce transits, and P_3 is the probability that a star that has a planet in an orbital plane on our line of sight will show three or more transits in the designated observation period.

For a given limiting magnitude, only about half the stars near the galactic plane are dwarfs. Many of the rest are giants, which are too large to have short-period planets or to show a detectable signal. Thus only one half of the field stars can be considered as targets so Pd ~ 0.5.

Observations of solar-like stars by Mayor and Queloz, 1995, Butler et al., 1997, Cochran and Hatzes, 1997, Noyes et al., 1997, and Marcy and Butler, 1998, have shown that approximately 1 to 2% of their target stars have giant planets with periods between three and six days (Marcy, private communication 1999). For those planets with orbital periods near 5 days, the probability that the orbital plane is near enough to our line of sight to show a transit is about 10%. (The slight increase in this fraction for the inclusion of planets with longer periods is ignored because of the small chance of observing the necessary three transits to recognize these events.) Hence Pp ~ 0.01 and Pa ~ 0.1.

The value of P_3 was estimated from a numerical simulation. The simulation assumes that the observations were made for a constant number of hours each night and that no nights were lost to bad weather. Transits are placed at all possible phases for periods between three and six days. Then the fraction of events for which three or more transits occurred is recorded as a function of the number of nights of observations. The results are shown in **Figure 1a**. From this figure it can be seen that during the summer when night time durations average about six hours, nearly six weeks of observations are required to produce a 65% chance of detecting three or more transits by a star that is presenting transits. In the winter, the situation is much better in that six weeks of observations produce a 80% chance. Only star fields that are well away from the ecliptic can provide such long durations. Thus the product of probabilities (i.e., the probability that a given star will show at least three transits) varies from 3.2×10^{-4} in the summer to 4.0×10^{-4} during the winter.

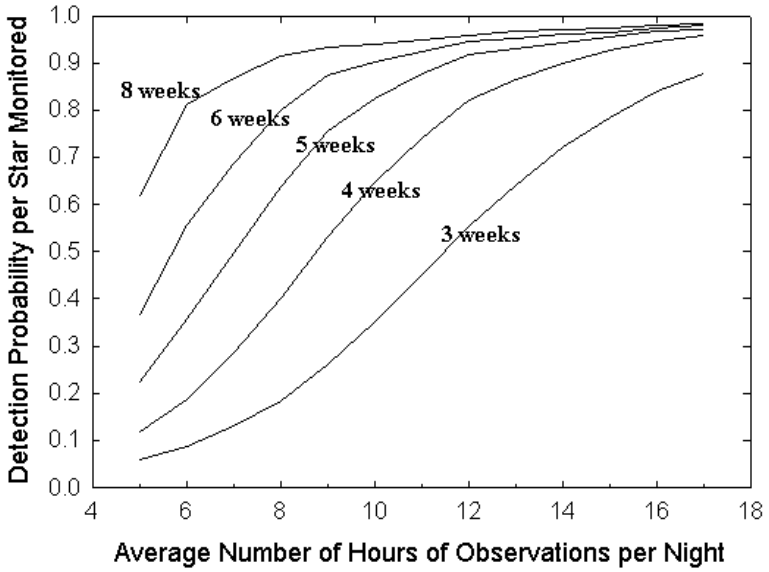

Figure 1a. The probability of detecting three or more transits for various choices of the length of night and the duration of the observations.

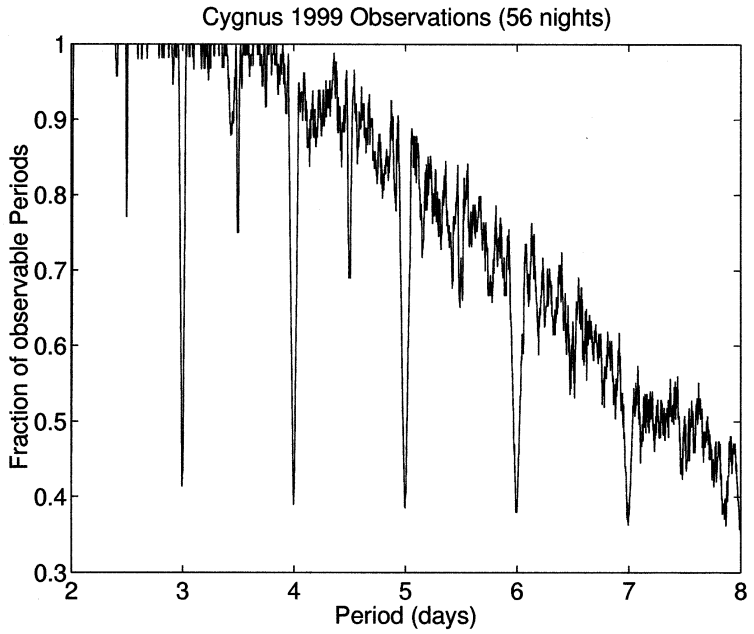

Figure 1b. The fraction of observable periods as a function of the orbital period for the 56 nights of observations of the Cygnus star field during the 1999 observation season.

Figure 1b shows that the actual probability is a function of the orbital period of the planet. For this calculation we used the actual data for the observations made in 1999 of the Cygnus star field. It is clear that for periods less than 4 days, the probability exceeds 0.9 and for orbital periods near 6 days, the fraction is near 0.7. These values are similar to those in **Figure 1a** for 8 weeks when the observations are conducted for 5 to 8 hours per night. Notice the large dips in the fraction of observable periods for integer and half-integer values of the period in days.

The yield is defined to be the product of the probabilities times the number of stars monitored , i.e., about 1.9 and 2.4 planets when 6000 stars are monitored for a six weeks during the summer and winter, respectively. For this calculation only the number of nights that are clear enough to achieve the required relative precision can be considered. Given the very real problems of bad weather and instrument down-time, this requirement often means that two to three calendar months will pass before the required number of nights is obtained. Nevertheless, observations of three rich star fields per year are practical. Thus about six planets should be discovered each year under these observing conditions.

INSTRUMENT DESCRIPTION

The Vulcan photometer is constructed from a 30 cm focal length, F/2.5 AeroEktar reconnaissance lens and Photometrics PXL16800 CCD camera. The lens is rigidly mounted in an aluminum box which also contains a digital micrometer stage that holds and moves the CCD camera as required for focusing. **Figure 2** shows a design schematic of the photometer. A spectral band-pass filter is placed between the shutter and the front window of the detector. Mounted on the top of the photometer are two small finder telescopes and the autoguider with Celestron Pixel 255 CCD. See **Figure 3**.

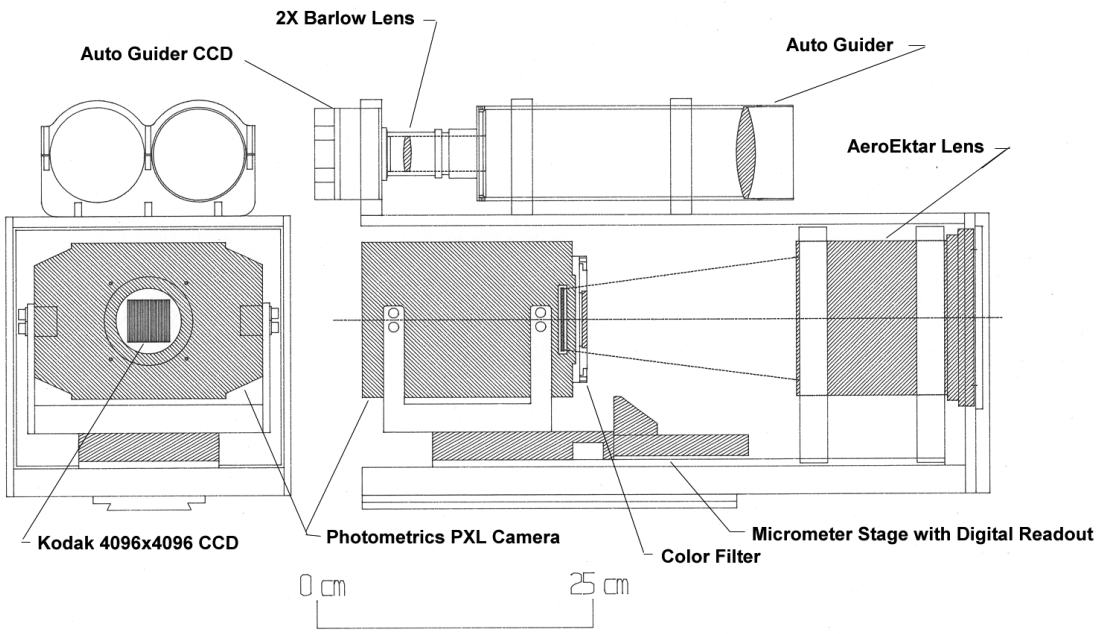

Figure 2. Schematic Drawing of the Vulcan Photometer

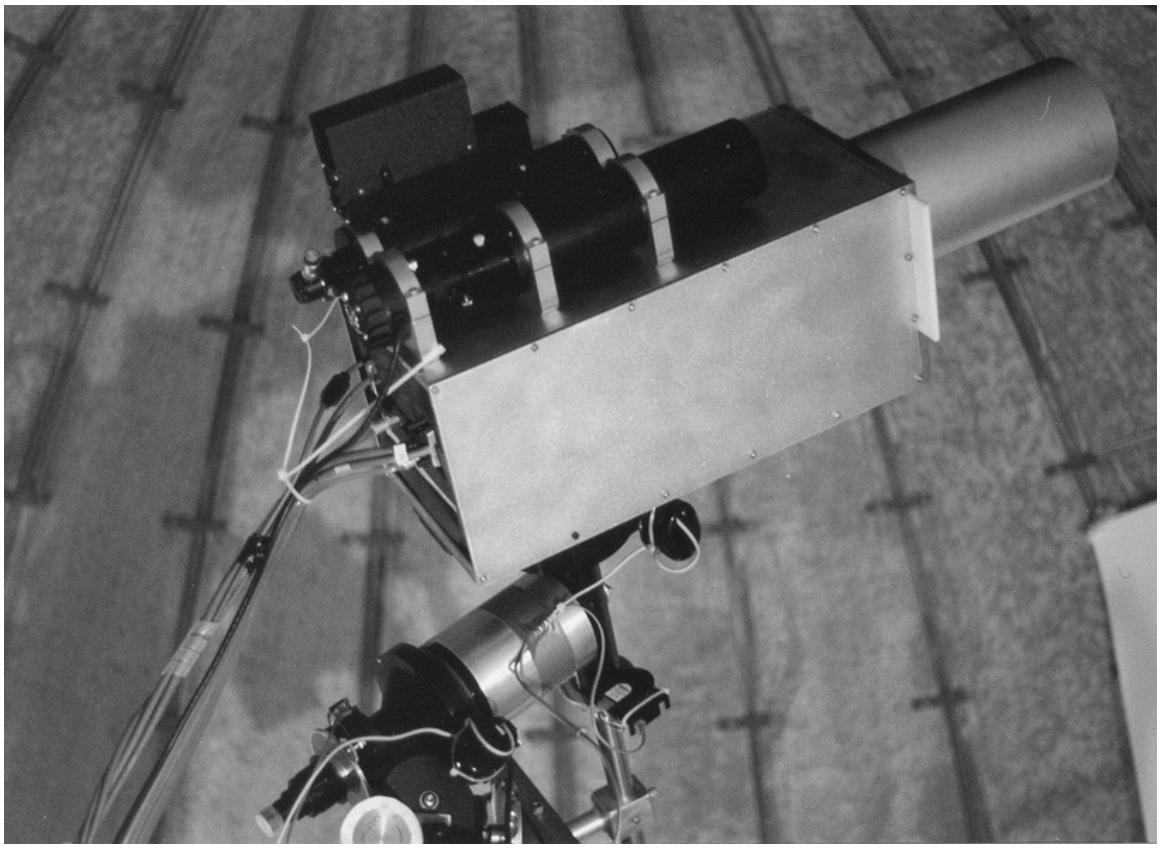

Figure 3. Photo of the Vulcan Photometer in the Crocker Dome. At the top are two finder scopes and auto guider. The white rectangle at the base of the tubular light baffle is the diffuser plate used for flat field calibration.

To minimize structural flexure and the differential motion between the auto guider and the main camera, the auto-guider was built from a 8 cm aperture 30-cm focal length lens and 2x Barlow lens that gave an effective focal length of 0.6 meters. Because the auto-guider focal length is twice that of the main camera and because the autoguider pixels are 7 μm instead of 9 μm, auto-guider errors of 1 pixel contribute less than 0.4 pixels to the motion of the star field on the main camera CCD. Thick brackets hold the short tube, Barlow lens, and the auto-guider at three points along its length directly to the base plate. To avoid the necessity of flipping the telescope when it had crossed the meridian, the mounting was modified to move the telescope away from the pedestal and the counter weight was shifted toward the pedestal to balance the torque of the forward-mounted camera.

A custom-designed filter that covers the spectral range associated with both the "V" and "R" bands of UBVRI photometry was chosen to maximize the optical throughput while avoiding problems in the blue and red portions of the spectrum. The transmission curve is shown in **Figure 4**. At short wavelengths, there are rapid changes in extinction with changes in air mass that are mitigated by rejecting flux at wavelengths shorter than 480 nm. In the red portion of the spectrum, emissions from the sky background can be reduced rejecting flux at wavelengths longer than 763 nm. The pass band is also helpful in reducing the chromatic aberration of the AeroEktar lens.

Measurements of the performance of the AeroEktar lens show that it transmits only about 45% of the incident light near 600 nm and that it has a point spread function with very broad wings. Because the appropriate star fields are in the galactic plane and somewhat crowded, it is helpful to use a tighter PSF to avoid background stars and to minimize the noise introduced by the sky background. An study of the lens by Tim Brown (High Altitude Observatory, UCAR, personal communication, 1999) suggested that PSF could be improved without dramatically reducing the light in the star image by an aperture stop. **Figure 5** shows our measurements of the encircled energy as a function of image radius for the lens used in the Vulcan photometer for the full aperture lens and for the lens stopped to F3.8. Fifty percent of the flux is confined to a radius of 3.5 pixels (21") for the lens stopped to F3.8 while the unstopped lens requires a 4.4 pixel (26.4") radius. Thus the stopped lens confines the flux to a core approximately 0.6 area of the unstopped lens. All data obtained after to May 3, 1999 used the stopped lens. The large star images have the disadvantage of providing modest contrast against the background illumination from the sky. However they are large enough to be over-sampled and thereby accurately fit by a PSF. Further, the PSF is not affected by seeing nor changes in the seeing that occur during the night.

The 49 sq. degree field of view (FOV) that is obtained by using a 37 mm square CCD detector and a 300 mm focal length lens is very advantageous for simultaneously monitoring a large number of bright stars. Nevertheless, the FOV is so large that corrections for the scale changes and motions introduced by differential refraction must be done for each image before the photometry can be done. For example, in the Cygnus field, when the stars in the corner of the FOV nearest the horizon are at airmass three, the

differential refraction relative to stars in the center of the field is 27” (4.5 pixels). For those stars at the other corner of the FOV, the change in relative position is 19” (3.2 pixels). When the stars are near the meridian, the differential displacements at the corners shrink to about 5”. The small component of the image motion that can be represented by field rotation as the field moves from horizon to horizon is position dependent but is usually less than two pixels. Thus changes in the differential refraction cause significant and non-linear plate scale changes throughout the night.

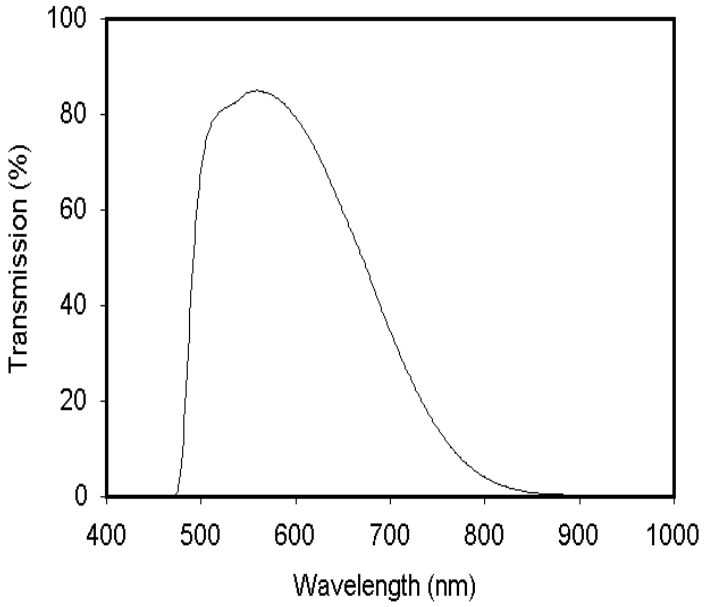

Figure 4. Transmission of the Color Filter

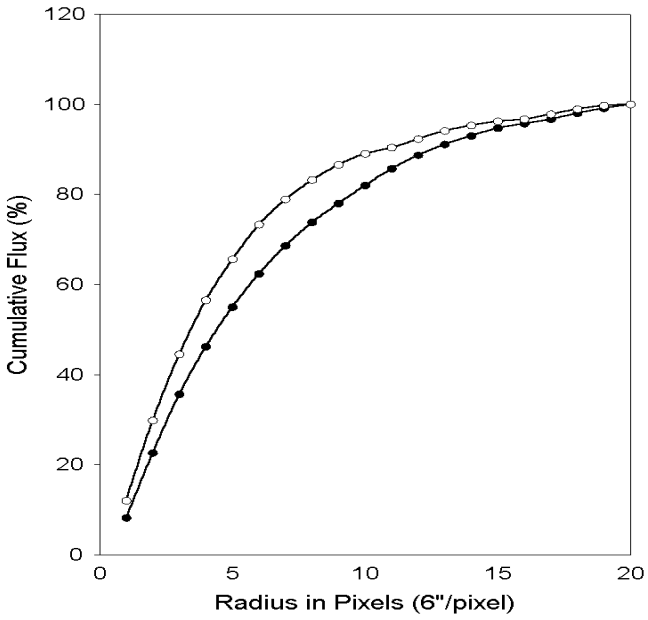

Figure 5. Effect of Aperture Mask on the Encircled Energy versus Image Radius for the AeroEktar Lens. Solid symbols represent the performance without a mask while the open symbols represent the effect of using an aperture mask.

The CCD detector in the main camera is a Kodak 4096x4096 format front-illuminated CCD with 9 μ pixels that is mounted in a Photometrics PXL 16800 camera. The detector is thermo-electrically cooled to –26.3 $\pm$0.2 ^{o}C. Because the data are read out as 16-bit numbers, each image file is 32 MB in size. The large size of the files demands that the computer controlling the camera and recording the images use a 32 bit operating system and 32 bit software. Because of the rarity of 32 bit software to control the camera and to display and record the results, a beta version of "V" Software (of the Photometrics Corporation) is used. Exposures are 7.5 minutes long and include a 30 second period for reading out the data to hard disk storage. The exposure time is short enough to avoid saturating ninth magnitude stars, but long enough to keep the amount of data to a manageable size. During an eight hour night, about 2 Gigabytes of data are recorded and then archived to CD-ROMs. This data set includes files for dark, flat, and bias frames.

For calibration purposes, several exposures are made each evening and morning to measure the bias level, the dark current, and the flat field correction. The bias signal has been found to be nearly constant during a single night. Because the detector is run in the MPP mode and because of the constant temperature maintained by the controller, the dark current is generally small and constant. As only a single exposure time is used for all the images, only one exposure is needed for the dark current measurements.

Flat field calibrations are obtained by pointing the photometer toward a white diffuser screen attached to the dome and illuminated by a high-temperature halogen lamp. To

avoid focussing the white calibration screen onto the detector by the short focal length objective, a translucent diffuser plate is placed just in front of the lens.

The photometer is housed in the Crocker Dome on Mt. Hamilton at Lick Observatory at an altitude of 1.3 km. The photometer is operated every clear night by a single member of a five-person team. So that a large number of target stars can be observed simultaneously, star fields along the galactic plane are monitored. A given field is monitored from dusk to dawn until several weeks of useful observations are acquired. This procedure provides maximum time coverage of the target stars and avoids wasted time due to slewing to new fields.

DATA PROCESSING

Because the goal of the Vulcan observations is the detection of extrasolar planets in inner orbits around dwarf stars, the methods employed to do the data analysis have been modified from the classical methods used in all-sky photometry and for relative photometry. Standardized all-sky photometry is best done by using photomultiplier tube detectors and special color filters and by comparing the target stars to standard stars. From such measurements, transformation coefficients are found that allow the transformation of the target star fluxes to those that would be measured with a "standard" system. When CCD detectors are used, accurate transformations to the standard system are very difficult. Further, Young et al., 1991 has shown that the equations upon which the transformations are based introduce significant errors. Relative photometry is less demanding in that the observations are made with reference to nearby stars of similar spectral characteristics rather than the set of "standard stars". Since the comparison stars are chosen to be similar to the target star and to be nearby, correction for extinction is usually not needed.

Our goal does not require that we make an accurate[2] determination of the brightness of stars relative to either standard stars nor to nearby comparison stars, but requires only the measurement of the short-term **changes** in the relative flux that occurs during a transit. We call our procedure "differential relative photometry" because of its similarity to relative photometry whereby the flux of a target star is measured relative to nearby comparison stars. Unlike the typical protocol used to do relative photometry, our method requires that corrections must always be made for extinction and these must be measured for every star on every night. This is necessary because the amplitude of the flux change due to a transit is small compared to the flux change that occurs because of the continuously varying air mass. Since thousands of stars in the same field of view are measured simultaneously and observed for many nights, it is straightforward to do a flux versus time correlation to find appropriate comparison stars for each target star. The extinction correction for the target star is always based on those measured for the group of comparison stars known to have extremely similar extinction behavior.

[2] We distinguish between accuracy and precision as follows; accuracy is measurement to an absolute standard whereas precision is the repeatability of the measurement without regard to whether the value is accurate.

However, there is no expectation that the same flux ratio of the target star to the group of comparison stars will be exactly the same from night to night. Small changes in the positions of the star images due to repositioning the telescope cause small changes in the output due to differing sensitivities of the individual pixels. These night-to-night changes are unimportant to the detection of the short transits that occur during a single night.

Since the transit periods sought are of the order of three hours, detection demands the measurements be made frequently throughout the night, but only requires that the relative precision of the photometry be maintained over a single night. Even if transits occur several nights or weeks apart, our goal can be attained without establishing and maintaining the accuracy required to measure the time-invariant flux or flux ratio of the target and comparison stars. In this way, the method of differential relative photometry greatly reduces the need for long term stability and allows the emphasis to be placed on obtaining very high precision for hour-to-hour measurements.

Thus differential relative photometry differs from both all-sky photometry and relative photometry in that it does not require the use of standard stars (because no transformations to a standard system will be made), but requires a high cadence of observations throughout the night, nightly measurements of extinction, and continuous observations of nearby comparison stars.

The data processing pathway for Vulcan Camera images can be divided into several discrete steps: star field preparation, image calibration, image reduction, and transit detection. Each stage is dependent on results from the preceding steps, but otherwise can be carried out in any order, allowing for varying processing parameters or methods at any stage of the pipeline.

The first step is performed once for each star field. It consists of selecting stars to be monitored and preparing an initial catalog file of each star's position and brightness on a reference frame. The stars are located on a single low-airmass image from a clear moonless night. The image background is found by fitting a polynomial surface to median values of small subsections, each approximately 350 pixels on a side. The flattened image is then correlated with a model Point Spread Function (PSF), currently a weighted average of a night's worth of images for an isolated star. Due to variation of star PSFs across the image, the frame is divided into nine (3 x 3) subframes. The background-subtracted subframes are each associated with a model Point Spread Function (PSF) that is produced from the weighted average of all the images from a single night for an isolated star in the subframe. The result of this two-dimensional correlation is a map of coefficients describing how well each point matches an isolated star. A threshold is applied to this map and all adjoining pixels that have values above the chosen threshold are identified as a star.

When the threshold is found by demanding a correlation coefficient above 0.8, about 9500 stars are found in each of two Galactic plane fields. This method selects a subset of stars which have an isolated star PSF (i.e. no "significant" overlap from another star's PSF). Thus, even though most of the chosen target stars are in crowded star fields, the chosen targets are not crowded. Because non stellar objects will also have a poor match

to the standard PSF, they too are eliminated as targets. Stars that are near the edges of the CCD, or near saturation are then eliminated from the list. Equatorial coordinates for the selected stars are determined from a third order plate transformation based on coordinates of known stars spread throughout the field. Results from this procedure consist of a list of star positions (both pixel row and column, and right ascension and declination), approximate visual magnitude, and catalog associations.

The second step is the generation of nightly and seasonal calibration images. We normally take several bias, dark, and flat frames each night. These images are combined to generate an average bias, dark, and flat for each night. We also create master calibration images from the average of all of the nightly files. These low-noise images are used when there is little night-to-night variation in the calibration images.

The third step in the processing pipeline is the systematic reduction of images. Our reduction package processes all images from a single night at one time, but several nights can be done in batch mode. The steps taken in the reduction of a night's images to light curves are as follows;

1. Individual images are corrected with dark and flat images, and the pixel values are corrected for non-linearity. The corrected frame is then registered with the reference frame to locate the target stars. The region around each target star that is large enough to contain both the star's PSF and to compute the background is saved to disk. This process is repeated for each image taken during the night.
2. For a small number of bright stars (of order 100), a PSF-fitting algorithm is used to solve iteratively for a PSF model specific to each star. The sub-pixel position and brightness of each star in each frame is then determined. A second order coordinate transformation is fit to the measured motions. Then the motion field is evaluated for each star to locate it on the data frame.
3. The interpolated motions are used to reduce the PSF-fitting problem to a simple least-squares problem, where the flux of each star in each frame is the only unknown parameter. The stars are then read into memory in batches of ~100. The star images are checked for energetic particle hits and outlying images. Particle hits are found by locating positive spikes in the time series of each pixel. Pixel values above a given threshold are replaced with the value from a polynomial fit to the time series. The threshold and polynomial order were determined empirically, but are user adjustable. Outlying star images are those for which the flux estimates differs substantially from the other estimates for that night. If outlying star images are found, they are flagged and not used in the PSF model for that star for that night. The star fluxes are fitted to the model PSF determined for each star from the night's images. The fluxes are then stored to disk along with supporting data including backgrounds, star positions and widths, and shot-noise estimates for each star.
4. The raw fluxes generated in step 3 must be corrected for extinction. To get a first estimate of the out-of-atmosphere value for each star, the extinction coefficients for photometric nights are calculated from $F(X) = F(0)*10^{-aX}$, where, F is the star flux, X is the air mass, and _ the extinction coefficient for each star. After removal of those stars found to have large night-to-night variations, comparison stars are found by computing the variance of the transmission difference between each nearby star and the target star for several photometric nights. The brightest ten (non-saturated) stars

are then chosen for the ensemble. This procedure guarantees that only non-variable stars with similar "color" are used as comparison stars. The average transmission determined on each frame for the ten comparison stars is used to determine the out-of-atmosphere value for each target star.

5. Each star's extinction-corrected flux is divided by the average of its extinction-corrected comparison stars. A list of variable stars and stars which show a high level of scatter is kept for each star field. This list contains both stars that are truly variable and those that show significant variation on the night they were processed due to the presence of artifacts such as contamination due to light from aircraft and satellite over flights. These stars are not used in the extinction correction fit in step 4, nor in the differential photometry normalization.

The final step in the Vulcan data processing pipeline is an automated search of the light curves for transit signatures. Detecting transit signals is a classical signal-detection problem for deterministic signals in colored noise (Van Trees, 1968). Essentially, the optimal detector whitens the observations and then correlates the whitened data with the signal resulting from passing a transit through the same whitening filter. Folding the time series at the orbital period of a planet coherently adds the test statistics for the bin containing the transit. The test statistics add incoherently if the wrong period or bin is chosen. The detection rate depends on the SNR of a single event, the number of events, and the detection threshold.

The light curves are first processed to remove outliers and the effects of systematic errors that might otherwise perturb the results. Isolated outliers are identified by quantifying the effect of each sample on the variance of all the samples collected on the same night about a trend line fitted to the night's data. Individual samples contributing more than a user-specified fraction of the night's variance are removed from the light curve. This process is iterated a few times. After isolated outliers are removed, systematic errors are detected and removed from the light curves by decorrelating each light curve against all other light curves over the entire data set using the procedure described in Jenkins et al. (2000). This technique removes structures that are highly correlated across multiple lightcurves while preserving structures that are unique to individual ones. The final step of preconditioning is the removal of an estimate of the mean flux for each night's observation from each lightcurve sample. Here, the estimate used was the sample at the 60% position of all samples when the night's samples were ordered in ascending brightness. (The50% sample represents the median of the set.) This choice tends to detrend light curves of eclipsing binaries and transits of 51-Peg like planets better than the sample mean or median when the sample-sample precision is much better than 1%. The resulting residual light curves are then subjected to a matched filter seeking transits with durations between two and four hours and periods between one and twelve days. The matched filter is implemented by convolving each light curve with a single prototype transit pulse and then folding the resulting single-transit statistics at each trial period. The results are normalized by the standard deviation of the light curve and the square root of the energy of the periodic transit pulse, accounting for the effects of missing data. The maximum test statistic is recorded for each star, as well as the maximum single transit test statistic. The

stars are ordered by the maximum test statistic in descending order for manual examination. In addition, a Lomb periodogram analysis is performed for each star to identify short-period eclipsing binaries and other periodic variable stars as well as to provide additional information for the manual examination of the light curves. Light curves which have high maximum test statistics are then subjected to further scrutiny.

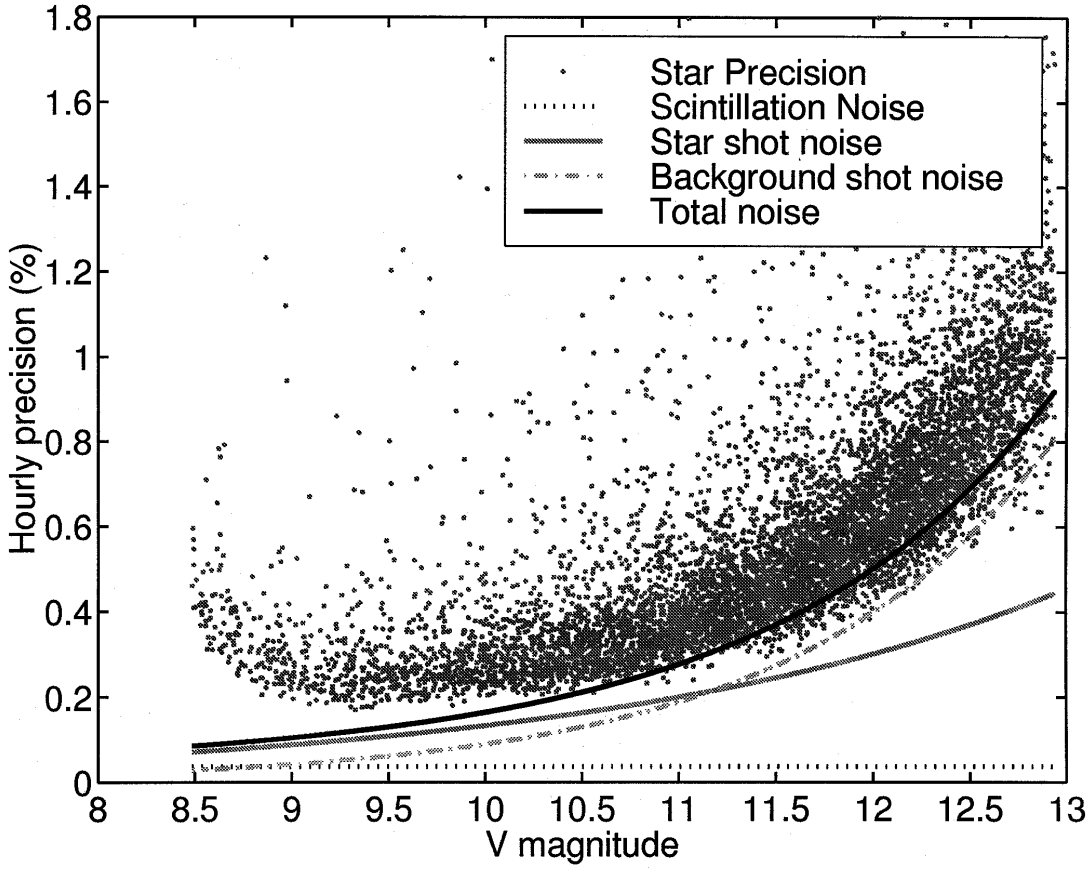

Figure 6. Measured and Predicted Precision vs. Stellar Magnitude. The upper solid curve represents the sum of the predicted scintillation and shot noise due to both the star and background. The lower solid curve represents the shot noise from the stellar flux and the dash-dot curve shows the predicted shot noise from the sky background. The horizontal dotted curve is the predicted scintillation noise for an airmass of 2.6. Stars brighter than 9th magnitude have lower precision due to the presence of saturated pixels.

CURRENT DIFFERENTIAL RELATIVE PHOTOMETRIC PRECISION

To determine the differential relative photometric precision that can be obtained with the photometer, a star field in Cygnus was observed for several hours on a photometric night. The results are shown in **Figure 6**. The horizontal line (dotted) is an estimate of the maximum noise introduced by scintillation and is calculated (Young, 1974, Dravins et al.,

1998), for an air mass of 2.6. Because most observations are usually made at a much lower air mass, this value is an upper limit. The bottom curve (short dashes) is an estimate of the shot noise introduced by the background which must be subtracted from the stellar flux. For stars dimmer than visual magnitude 11.6, this adds a larger noise contribution than does the shot noise from the star itself. The high background level is caused by the large area (36 square arc seconds) of the sky that is imaged onto each pixel by the short (30-cm) focal length camera lens. It would be an even greater noise source if the detector had larger pixels. The curve marked with long dashes is an upper-limit estimate of the total noise expected from all three noise sources. The topmost curve is a fit to the measured median hour-to-hour absolute deviation. The median is used here to avoid the large bias introduced from occasional outliers.

It is clear from a comparison of the data from predicted and measured precision for stars brighter than 11^{th} magnitude, that the noise introduced by the shot noise of the stars themselves is not a limitation, i.e., the small aperture is not the major limitation to the precision obtained here. Hence, another source of error must exist that is at least as important as those already discussed. An investigation was conducted to identify the other noise sources.

IDENTIFICATION OF PROCESSES THAT LIMIT PHOTOMETRIC PRECISION

Another potential source of noise is the overlapping of star images in the crowded fields. Because of the need to simultaneously monitor many stars, most of the chosen star fields are in or close to, the galactic plane

A study was conducted of two portions of the Cygnus star field to determine if the measured photometric precision was related to the area density of stars, i.e., crowding. No significant correlation was found. This lack of correlation is probably due to the criterion that is applied to the original selection of target stars from the totality of the stars in the field-of-view of the reference frame. For a star to be selected as a target, it must show a good fit to a pre selected PSF. This procedure eliminates overlapped stars, stars with bright neighbors, and non-stellar objects.

Small motions of an image across a CCD detector can cause large changes in the output because of the both intra- and inter-pixel variability (Buffington et al, 1990 &1991, Robinson et al, 1995). Because of the potential importance of this noise source, extensive tests are underway to quantify the effect of image motions and to distinguish them from the effects of secular trends. It is also possible that the psf-fitting procedures are not adequate. (See the discussions in Howell, 1989 and Stetson, 1990.)

RESULTS OF EXAMINING THE LIGHT CURVES FOR 6000 STARS IN THE CYGNUS STAR FIELD

A seven by seven degree field centered at RA and DEC of 19hr 47min, $+36^{o}$ 55’ was observed in 1998 from August 10 through September 30. Useful data were obtained on twenty-nine nights. Nearly fifty stars showed some evidence of transits with periods

between 0.3 and 8 days. Most had large amplitudes like the examples shown in **Figure 7** through **Figure 10**. Except for the very unlikely situation where the primary was later than spectral type M0, the amplitudes are too large to represent planetary transits. Further, the durations are also much longer than that expected from a planetary transit. The obvious presence of a secondary transit in all the figures confirms the multiplicity of the systems. Note that if the amplitudes of the primary and secondary transits in **Figure 9** were slightly more equal, then it would be difficult to distinguish the two transits at half the real period from a single transit of a dark companion at that period. However, a small, dark companion can often be distinguished from two nearly identical stars that are showing grazing transits because of the "V" shape of the latter's transit compared to the nearly constant amplitude of the former.

Several stars showed low amplitude transits as for example, in **Figures 11 and 12.** The data for these two stars has been folded and binned into 30 minute periods. The mean deviation for the binned points is about 0.1% when several data strings are folded for the purpose of discovering low amplitude transits. Hence, transit amplitudes of 1% to 2% from jovian-size planets can be readily detected. However when high-resolution spectra were obtained for both of these stars, they were found to be double-lined binaries so similar in size as to have indistinguishable transit depths. (Note that this fact implies that the photometric periods shown in the figures must be doubled). The low amplitude of the transits is explained if the stellar orbital planes are tipped from the line of sight by approximately 9 and 14 degrees (for stars #1433 and #937, respectively) causing both binaries to exhibit grazing transits. **Figure 13** shows the spectral region near the H_β line for star #937. Two absorption lines due to the Doppler-shifted H_β line are apparent.

Figure 14 is the folded and phased light curve for 3047. The transit depth is 3% with a period of 4.65 days. Radial velocity measurements by David Latham (personal communication, 1999) are presented in **Figure 15**. The Doppler velocity data indicate that the period is exactly the photometric period. The combined data were used to obtain a preliminary solution for the structure of the system. It showed the system to be a single-lined, high mass-ratio (4:1) binary with a primary of late-F spectral type and a secondary consistent with a mid-M spectral type dwarf.

In early November of 1999, two groups announced the discovery of a planet orbiting HD209458 in the Pegasus constellation (Charbonneau et al. 1999, Henry et al. 1999). At this time of the year, the predicted transits occur about the time the star sets as seem from Lick Observatory. Because the transit occurred about the time that the star set, the observations were necessarily made at unusually high air mass. The symbols shown in **Figure 16** shows the extinction-corrected, normalized light curve we obtained for HD209458 on that date. The solid line represents the predictions based on the work of Charbonneau et al. and Castellano et al. 2000. Both the limb crossing time (25 minutes) and the measured amplitude of the transit (1.6%) are consistent with those found by Charboneau et al. Our best fit to the time of onset of the transit is based upon the transit epoch from Charboneau et al. 1999 , but uses the orbital period derived from the Hipparchos observations of HD209458 by Castellano et al. 2000.

Ordinarily, photometry is done as close to the meridian as possible to mitigate the error introduced by scintillation and rapid extinction variations that are associated with high air mass. For this reason, measurements are usually made at air mass less than 1.5 and seldom made at an air mass as large as 2.0. Because the November 22 event was the last opportunity to observe the transit, observations were made even though the air mass ranged from 1.5 to 4 during the measurements. **Figure 17** shows the measured rapid increase in standard deviation (SD) of the fluxes of the seven comparison stars at the time of the measurements. The solid curve shows the expected level of scintillation noise (Young, 1974). The agreement between the measurements and the predictions demonstrates that the system was operating at a precision limited only by properties of the atmosphere. The observations were terminated at an airmass of four because the signal to noise ratio had dropped below 2.5 at that point.

A comparison of the light curves of the comparison and target stars is shown in **Figure 18**. The dashed curves represent the time variation of flux from the seven comparison stars whereas the solid curve shows the variation from the target star HD209458. It is clear that although the scatter of the measurements grows rapidly with time, the time variation of the target star is distinctly different than those of the comparison stars. These observations are in excellent agreement with the predictions of Charbonneau et al. 1999.

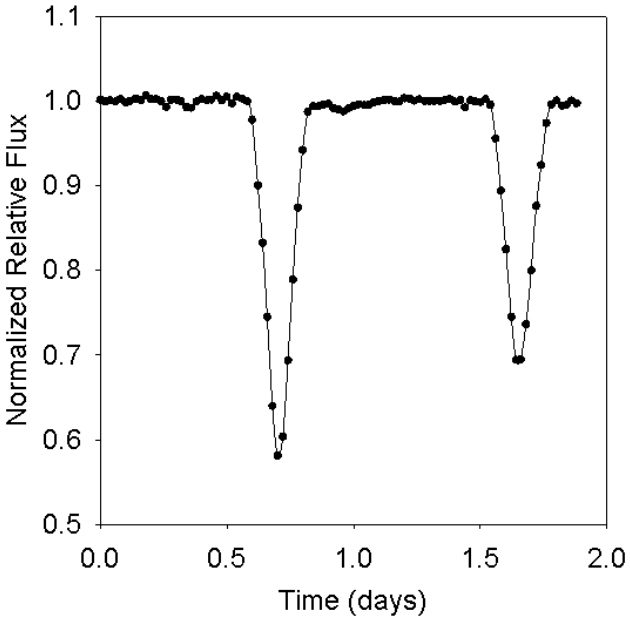

Figure 7. Star #805 with a period of 1.9 days and dips of 60% and 30%.

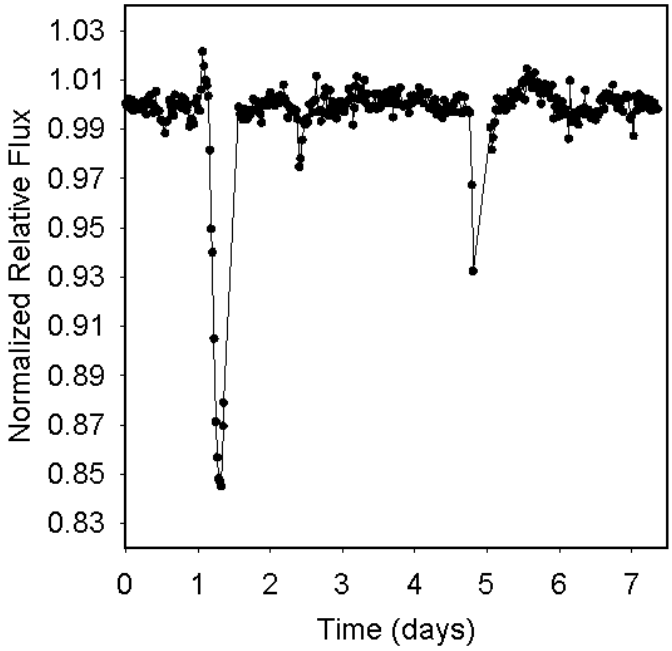

Figure 8. Star #1918 with a period of 7.17 days and amplitudes of 15% and 6%.

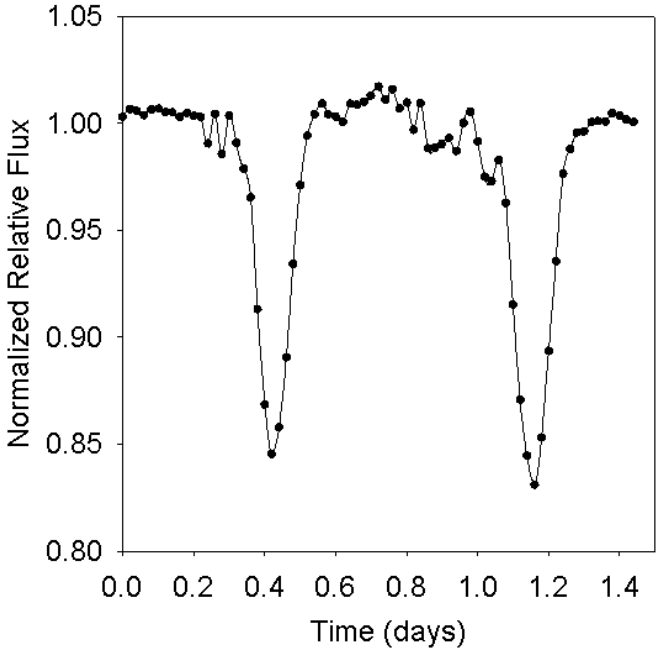

Figure 9. Star #874 with a period of 1.44 days and amplitudes of 16% and 17%.

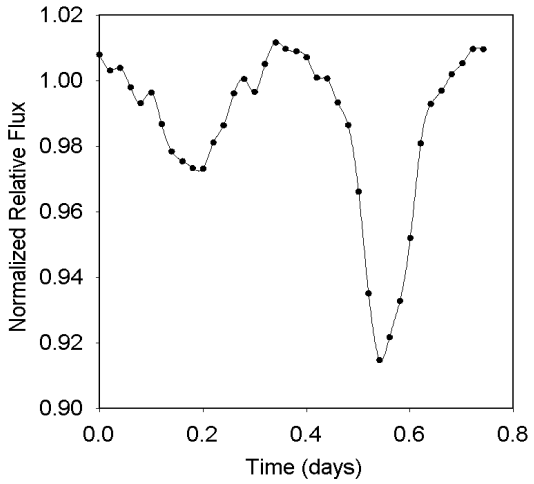

Figure 10. Star#3731 with a period of 0.7598 days and amplitudes of 9% and 3%.

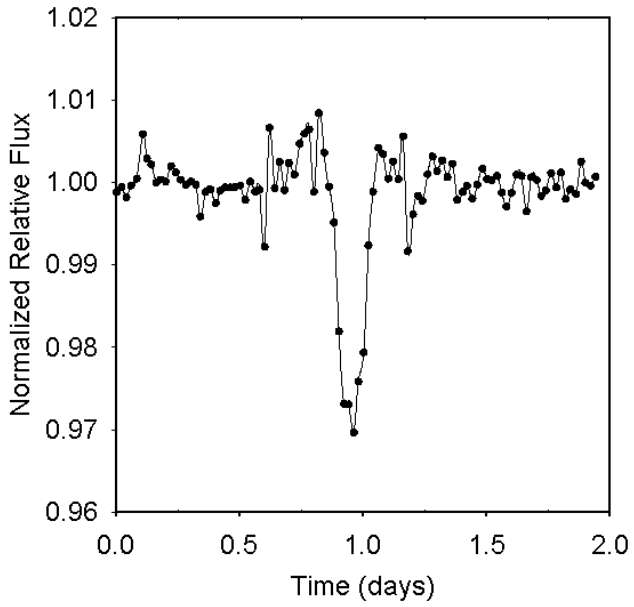

Figure 11. Folded and Phased Light Curve for Star #1433. Note that the actual period is twice what is shown here.

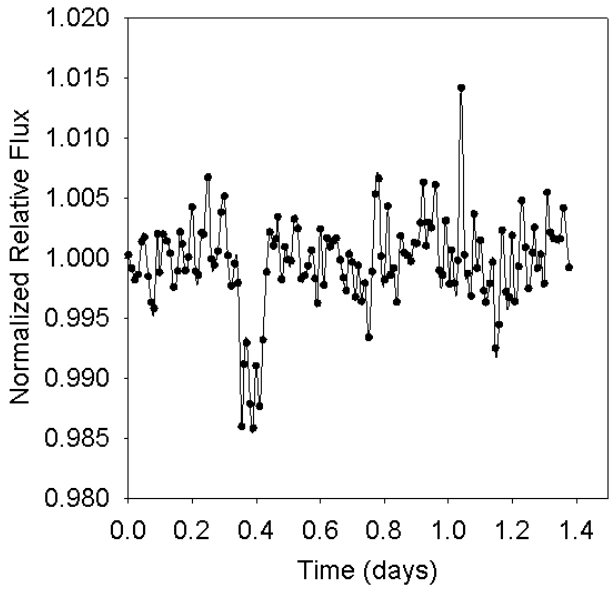

Figure 12. Folded and Phased Light Curve for Star #937. Note the absence of a second dip and the very low amplitude of the transit (1.3%). Note that the actual period is twice what is shown here.

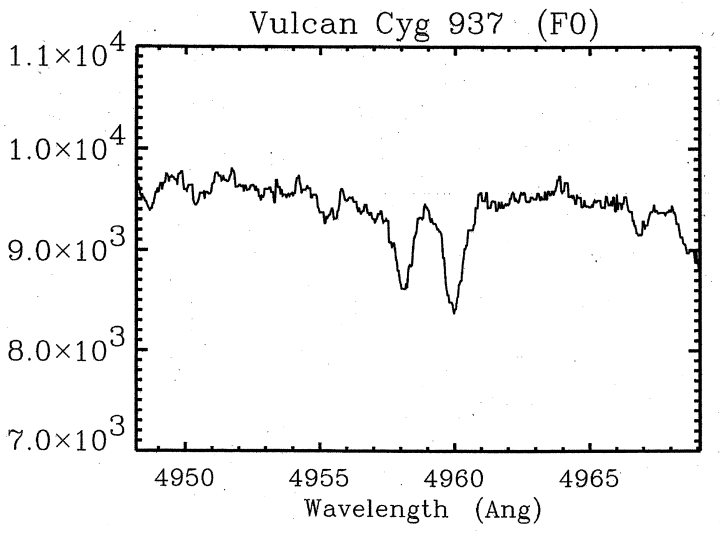

Figure 13. Spectra near Hβ line of Star #937. (G. Marcy, P. Butler, & J. Lissauer, personal communication, 1999)

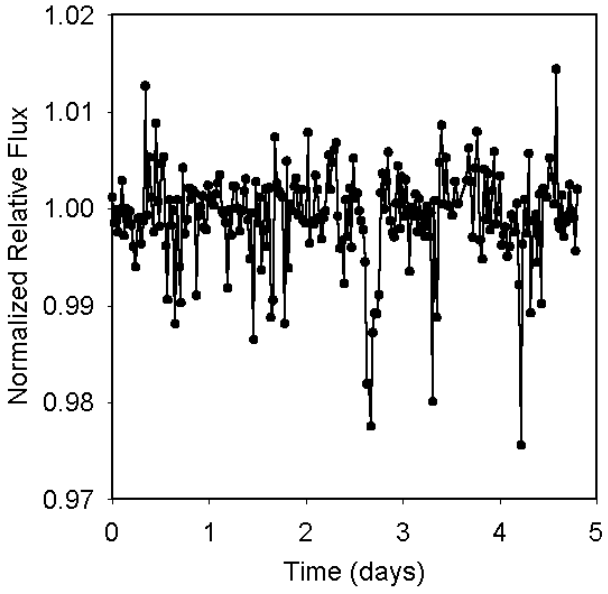

Figure 14. Folded and Phased Light Curve for Star #3047.

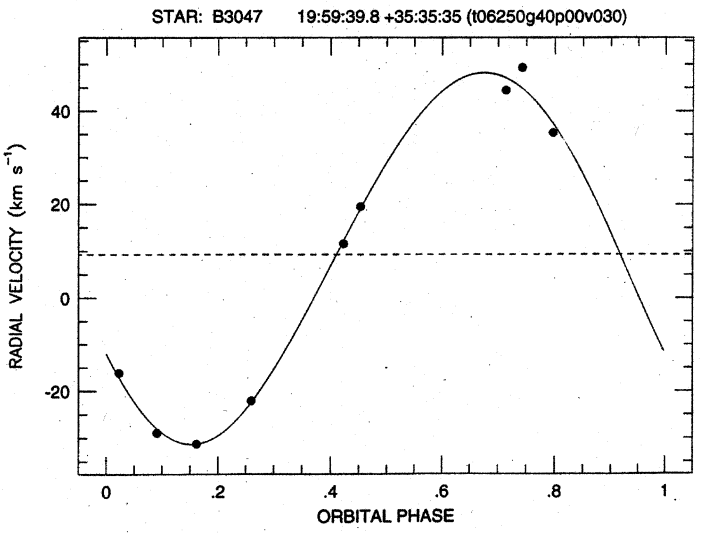

Figure 15. Doppler Velocity Measurements (Latham et al., personal communication, 1999) for Star #3047.

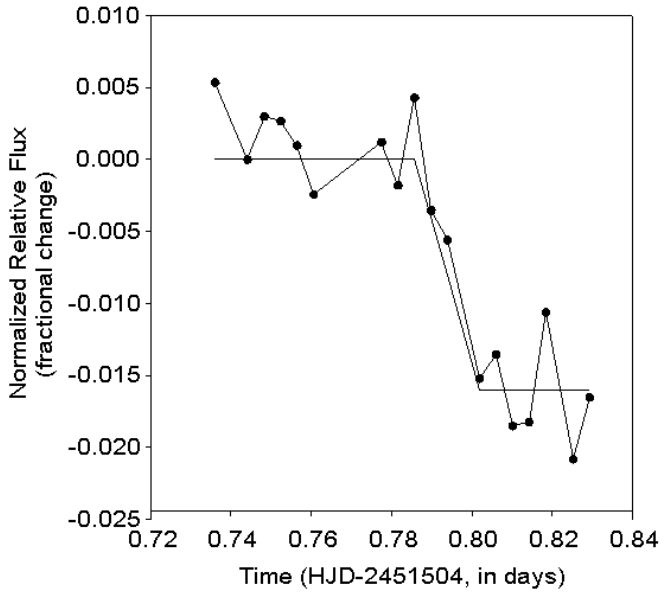

Figure 16. Comparison of the Measured and Predicted Flux for the November 22, 1999 Transit of a Planet Orbiting HD209458.

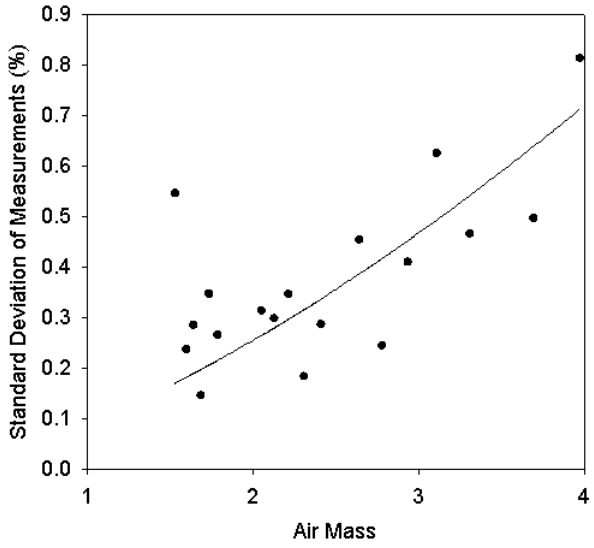

Figure 17. Comparison of the standard deviation of the fluxes of the comparison stars with the prediction of scintillation noise by Young (1974).

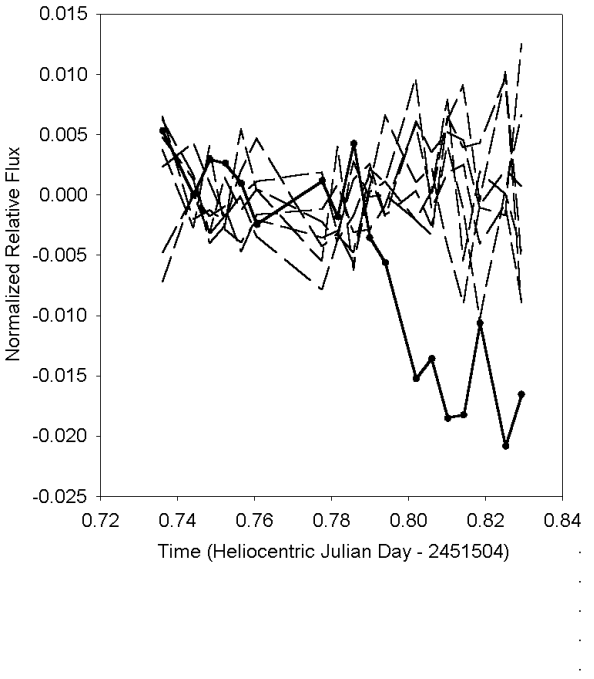

Figure 18. Measured Fluxes of Comparison Stars and HD209458 versus Time. (Dashed lines represent the comparison stars and the solid line represents the time variation of HD209458.)

CONCLUSIONS

A small photometer to detect extrasolar planets has been constructed and tested. It simultaneously monitors 6000 stars in star fields in the galactic plane. A method of differential relative photometry is used to maximize the precision of hour-to-hour samples. When the data are folded to discover low amplitude transits, stars showing repeated transits with depths of 1% or more are readily detected. This precision is sufficient to find jovian-size planets orbiting solar-like stars, which have signal amplitudes from 1 to 2% depending on the inflation of the planet and the size of the star.

Complex data processing of the images is necessary to compensate for the motions of the images due to imperfect polar alignment and differential refraction. A polynomial coordinate transformation of each image is required to correct the nonlinear scale changes and rotation that occur during the night. The numerical overhead for the PSF-fitting is greatly reduced by first solving for the motions of a subset of stars, and then interpolating the motions across the field. . This method provides an efficient, single parameter, linear least squares approach to determining the flux of each star in each image. For the most well-behaved stars, the seven minute, image-to-image relative precision is about $3x10^{-3}$ before any period folding is done to reduce the noise. After data folding is done, the hour-to-hour precision sometimes reaches $1x10^{-3}$.

An investigation of possible noise sources indicates that star field crowding, scintillation noise, and photon shot noise are not the major noise sources for stars brighter than visual magnitude of 11.6. An investigation is underway to determine if image motion over the CCD detector is the major noise source.

Nearly fifty eclipsing binary stars have been found in the first star field of 6000 stars, many with transit amplitudes of only a few percent. Spectroscopic measurements were made on three stars that showed only one transit per period. Two of these were found to be nearly identical stars in binary pairs orbiting at double the apparent photometric period. One was found to be a high mass-ratio single-lined binary orbiting with the observed photometric period. The November 22, 1999 transit of a planet orbiting HD209458 was clearly observed at the predicted time and amplitude.

These results demonstrate that the Vulcan photometer and the associated data reduction and analysis techniques have the precision necessary to detect jovian-size planets orbiting solar-like stars.

ACKNOWLEDGEMENTS

The authors would like to thank the observers who spent many sleepless nights obtaining the data; especially Tim Castellano, Tony Dobrovolskis, Wendy Hansen, Carol Harper, Lynn Harper, Ralph Libby, Alan Meyer, Patrick Maloney, William Trublood. The superb work of the machine shop headed by Dave Scimeca was critical to the success of the project. Scripts to control and automate the operation of the camera were written by Bob Slawson of the Rochester Institute of Technology. John Caldwell, on sabbatical from

York University, investigated the influence of star crowding on photometric precision. Robert Yee directed system operation and maintenance. Kim Kubota (Orbital Science Corp.) and Walt Miller (Man Tech Corp) directed the observers. The cooperation and help of the Lick Observatory staff, especially Remington Stone, and their permission to use the Crocker Dome made the project possible. Special thanks are due to Geoff Marcy, Paul Butler, Jack Lissauer, Eduardo Martin, David Ardilla, and Dave Latham who made spectroscopic observations of candidate stars. Advice from Tim Brown (HAO, UCAR), Ted Dunham (Lowell Obs.), and Laurence Doyle (SETI Institute) contributed the success of the project. The patience, support, and funding received from Origins and Advanced Project Offices at NASA Headquarters and the Astrobiology Office at NASA Ames is gratefully acknowledged.

REFERENCES

Buffington, A., Hudson, H. S., and Booth, C. H. 1990, *PASP*, 102, 688

Buffington, A., Booth, C. H., and Hudson, H. S. 1991, *PASP*, 103, 685

Butler, P., G. Marcy, E. Williams, H. Hauser, and P. Shirts. Three new "51 Peg-type" planets. *ApJ Lett* 474, L115, 1997.

Castellano , T., J. Jenkins, D.E. Trilling, L. Doyle, and D. Koch, Detection of planetary transits of the star HD209458 in the Hipparcos data set. *ApJ Lett.* 532, L51 2000.

Charbonneau, D., T. M. Brown, D. W. Latham, and M. Mayor, Detection of Planetary Transits across a Sun-like star. *ApJ Lett.* submitted 1999.

Cochran, W., A. Hatzes, P. Butler, G. Marcy. The discovery of a planetary companion to 16 Cyg B. *ApJ.* 483, 457, 1997.

Dravins, D. L. Lindegren, E. Mezey, A. T. Young. Atmospheric intensity scintillation of stars. III. Effects for different telescope apertures. *PASP* 110, 610-633, 1998.

Frandsen, S., P. Dreyer, and H. Kjeldsen. Stellar photometric stability. *Astron. Astrophys.* 215, 287-304, 1989.

Gilliland, and T. Brown, Limits to CCD ensemble photometry precision, and prospects for astroseismology. *PASP* 104, 582-591, 1992.

Guillot, T., A. Burrows, W. B. Hubbard, J. I. Lunine, and D. Saumon. Giant Planets at small orbital distances. *ApJ. Lett*. 459, L35-L38, 1996.

Henry, G. W. , G. W. Marcy, R. P. Butler and S. S. Vogt, *ApJ Lett.* Submitted 1999.

Howell, S. B., Two-dimensional aperture photometry: Signal-to-Noise Ratio of Point-Source Observations and optimal data-extraction techniques. *PASP* 101, 616-622, 1989.

Jenkins, J. M., F. Witteborn, D. G. Koch, E. Dunham, W. J. Borucki, T. F. Updike, M. A. Skinner, and S. P. Jordan. Processing CCD images to detect transits of Earth-sized planets: Maximizing sensitivitiy while achieving reasonable downlink requirements. *SPIE* 4013, 520-531, 2000.

Lang, K. R., Astrophysical Data: Planets and Stars. Springer-Verlag, New York, 1992.

Marcy, G. and P. Butler P. Detection of Extrasolar Giant Planets. *Ann. Rev. Astron. Astrophys.* 36, 56, 1998.

Mayor, M. and D. Queloz. A jupiter mass companion to a solar-type star. *Nature* 378, 355-359, 1995.

Noyes, R. W., S. Jha, S. G. Korzennij, M. Krockenberger, and P. Niesenson. A planet orbiting the star rho Coronae Borealis. *Ap. J.* 483, L111, 1997.

Olsen, E. H., On the stability of the photometric system of the four-channel spectrograph-photometer on the Danish 50 cm reflector located on Cerro La Silla, Chile. *Astron. Astrophys.* 58, 217-220, 1977.

Robinson, L. B., M. Z. Wei, W. J. Borucki, E. W. Dunham, C. H. Ford, and A. F. Granados. Test of CCD Precision Limits for Differential Photometry. *PASP* 107, 1094-1098, 1995.

Stetson, P. R., On the growth-curve method for calibrating stellar photometry with CCDs. *PASP* 102, 932-948, 1990.

Van Trees, H. L., Detection, Estimation, and Modulation Theory, Part 1, John Wiley and Sons, New York, 1968.

Young, A. T., Methods of Experimental Physics, 12A (ed. N. Carlton) Academic Press, New York 1974.

Young, A. T., R. Genet, L. Boyd, W. J. Borucki, G. Lockwood, G. Henry, D. S. Hall, Pyper-Smith, S. L. Baliunas, R. Donahue, D. H. Epand. Precise automatic stellar photometry. *PASP* 103, 221-242, 1991.

List of Figure and Table Titles.

Table 1. Signal Amplitude vs. Stellar Type for Jovian-size Planets and Planets with Inflated Atmospheres

Figure 1a. The probability of detecting three or more transits for various choices of the length of night and the duration of the observations.

Figure 1b. The fraction of observable periods as a function of the orbital period for the 56 nights of observations of the Cygnus star field during the 1999 observation season.

Figure 2. Schematic Drawing of the Vulcan Photometer

Figure 3. Photo of the Vulcan Photometer in the Crocker Dome. At the top are two finder scopes and an auto guider. The white rectangle at the base of the tubular light baffle is the diffuser plate used for flat field calibration.

Figure 4. Transmission of the Color Filter

Figure 5. Effect of Aperture Mask on the Encircled Energy versus Image Radius for the AeroEktar Lens. Solid symbols represent the performance without a mask while the open symbols represent the effect of using an aperture mask.

Figure 6. Measured and Predicted Precision vs. Stellar Magnitude. The upper solid curve represents the sum of the predicted scintillation and shot noise due to both the star and background. The lower solid curve represents the shot noise from the stellar flux and the dash-dot curve shows the predicted shot noise from the sky background. The horizontal dotted curve is the predicted scintillation noise for an airmass of 2.6. Stars brighter than 9^{th} magnitude have lower precision due to the presence of saturated pixels.

Figure 7. Star #805 with a period of 1.9 days and dips of 60% and 30%.

Figure 8. Star #1918 with a period of 7.17 days and amplitudes of 15% and 6%.

Figure 9. Star #874 with a period of 1.44 days and amplitudes of 16% and 17%.

Figure 10. Star #3731 with a period of 0.7598 days and amplitudes of 9% and 3%.

Figure 11. Folded and Phased Light Curve for Star #937. Note the absence of a second dip and the very low amplitude of the transit (1.3%). Note that the actual period is twice what is shown here.

Figure 12. Folded and Phased Light Curve for Star #1433. Note that the actual period is twice what is shown here.

Figure 13. Spectra near Hβ line of Star #937. (G. Marcy, P. Butler, & J. Lissauer, personal communication, 1999).

Figure 14. Folded and Phased Light Curve for Star #3047.

Figure 15. Doppler Velocity Measurements (Latham et al., personal communication, 1999) for Star #3047.

Figure 16. Comparison of the Measured and Predicted Flux for the November 22, 1999 Transit of a Planet Orbiting HD209458.

Figure 17. Comparison of the standard deviation of the fluxes of the comparison stars with the prediction of scintillation noise by Young (1974).

Figure 18. Measured Fluxes of Comparison Stars and HD209458 versus Time. (Dotted lines represent the comparison stars and the solid line represents the time variation of HD209458.)